Acta Biomaterialia xxx (xxxx) xxx

Contents lists available at ScienceDirect

Acta Biomaterialia

journal homepage: www.elsevier.com/locate/actbio

Full length article

Spatiotemporal remodeling of bone as a reversibly adaptive biological material in Djungarian hamsters under regulated photoperiod conditions

Felix N. von Brackel [a,b], Praveer Sihota [a,b], Kathrin Mletzko [a], Johannes van Kaick [a,b], Johannes Krug [a,b], Xenia Junimann [a], Ceyda Cubuk-Charalampous [c], Maximilian Neidhardt [b,d], Alexander Schlaefer [b,d], Petar Milovanovic [e], Annegreet Vlug [f], Katharina Jähn-Rickert [a,b,g], Annika Herwig [h], Björn Busse [a,b,i,*]

[a] Department of Osteology and Biomechanics, University Medical Center Hamburg-Eppendorf, Lottestrasse 55a, 22529 Hamburg, Germany
[b] Interdisciplinary Competence Center for Interface Research (ICCIR), Martinistrasse 52, 20246 Hamburg, Germany
[c] Institute of Zoology, University of Hamburg, Hamburg, Germany
[d] Institute of Medical Technology and Intelligent Systems, Hamburg University of Technology, Am Schwarzenberg-Campus 3, 21073 Hamburg, Germany
[e] Center of Bone Biology, University of Belgrade - Faculty of Medicine, Dr. Subotica 4/2, Belgrade, Serbia
[f] Centre for Bone Quality, Leiden University Medical Center (LUMC), Leiden, the Netherlands
[g] Mildred Scheel Cancer Career Center Hamburg, University Cancer Career Center Hamburg, University Medical Center Hamburg-Eppendorf, Martinistrasse 52, 20251 Hamburg, Germany
[h] Institute of Neurobiology, Ulm University, Albert-Einstein-Allee 11, 89091 Ulm, Germany
[i] Materials Sciences Division, Lawrence Berkeley National Laboratory, 1 Cyclotron Rd., Berkeley, CA 94720, USA

ARTICLE INFO

Keywords:
Adaptive materials
Multiscale analytics
Structural materials
Biomechanics
Nature-inspired composites

ABSTRACT

Bone loss in humans is typically progressive and difficult to reverse, posing challenges for both pharmacological therapy and the long-term performance of bone replacement materials. Photoperiod-sensitive species such as the Djungarian hamster undergo cyclical physiological adaptations in response to seasonal light cues, providing a unique framework to investigate bone adaptation during physiologically regulated phases of bone loss under endocrine and circadian control without surgical or pharmacological intervention.

Female Djungarian hamsters were maintained under long-day (LD) or short-day (SD) photoperiods to induce physiological body weight loss without surgical or pharmacological intervention. Femoral and tibial bones were analyzed across mechanical, microstructural, and cellular scales using three-point bending, high-resolution microcomputed tomography, histomorphometry, and deep-learning–based quantification of bone marrow adipocytes.

Under SD conditions, bone exhibited reduced mass ($p = 0.001$), trabecular number ($p = 0.003$), cortical thickness ($p = 0.009$), and mechanical strength ($p = 0.013$), along with increased marrow adiposity ($p < 0.001$) and matrix erosion ($p = 0.020$). These changes occurred without surgical manipulation, reflecting a physiologically driven, photoperiod induced bone loss mechanism.

The Djungarian hamster provides a non-invasive framework model to study bone as a physiologically regulated biological material undergoing osteoporosis-like changes. By enabling photoperiod-controlled bone remodeling, this system offers translational opportunities to study bone material adaptation and the biological environment relevant for biomaterial performance under conditions of bone loss. Moreover, this model provides a physiologically relevant platform to study age- and endocrine-associated bone loss mechanisms and to inform the development of future osteoanabolic strategies.

Statement of significance: Bone loss caused by disease or disuse is typically progressive and difficult to reverse, and most experimental models rely on invasive surgical or pharmacological interventions to induce osteoporosis. In contrast, photoperiod-sensitive species such as the Djungarian hamster exhibit naturally regulated, potentially reversible skeletal adaptation. In this study, we characterize bone as a potentially reversibly adaptive biological material under controlled photoperiod conditions. Using multiscale structural, mechanical, and histological analyses, we show that short-day photoperiods induce pronounced, physiologically regulated changes in bone

* Corresponding author.
E-mail address: b.busse@uke.uni-hamburg.de (B. Busse).

https://doi.org/10.1016/j.actbio.2026.02.017
Received 8 October 2025; Received in revised form 15 January 2026; Accepted 11 February 2026
Available online 12 February 2026

microarchitecture, mechanical competence, and marrow composition without surgical manipulation. Understanding how bone adapts, deteriorates, and regains function under endogenous control may inform the development of regenerative materials and therapies capable of operating within dynamically changing and compromised skeletal environments.

1. Introduction

Bone loss in humans, caused by aging, disuse, or disease, is typically progressive and represents a major challenge not only for pharmacological treatment but also for the long-term stability and performance of implanted biomaterials [1,2]. Restoration of bone mass can be achieved pharmacologically using antiresorptive agents and, more effectively, anabolic therapies such as teriparatide or romosozumab [3,4]. In particular, while pharmacological treatments are well established, bone retains an inherent capacity to adapt to mechanical loading, exhibiting bone loss during disuse and bone gain in response to increased loading; however, these adaptive processes typically require strong or sustained stimuli. For example, changes in body weight, including increased adiposity or anorexia, are accompanied by corresponding adaptations in bone mass [5–7]. Interestingly, animals such as the Djungarian hamster exhibit a photoperiod induced body weight loss and gain [8]. Exposure to SD photoperiods induces a state characterized by prolonged melatonin secretion, gonadal regression with reduced sex hormone levels, voluntary reductions in food intake and locomotor activity, and a loss of up to ~30 % of body weight over several weeks [8–12]. These endocrine and behavioral changes are accompanied by the expression of daily torpor, a state of marked metabolic downregulation, resulting in substantially reduced mechanical loading of the skeleton. Together, this photoperiod-regulated cascade may influence the bone remodeling process through coordinated effects on metabolism, endocrine status, skeletal loading, and the associated cellular processes governing bone turnover. Importantly, these adaptations are induced solely by environmental light–dark cues, without surgical or pharmacological intervention, establishing the Djungarian hamster as a physiologically regulated model of accelerated bone loss.

This raises the question of whether, and to what extent, hamster bone is influenced by photoperiod induced changes in body weight but also by the underlying endocrine and circadian signals presumed to drive these adaptations. In the future, this model may enable studies aimed at understanding not only bone loss but also endocrine mechanisms that promote bone regain. Moreover, it offers the opportunity to investigate bone loss under physiological conditions without the need for surgical or pharmacological interventions. Additionally, this model may be of particular interest for studying how physiologically compromised bone environments influence biomaterial performance, stability, and long-term interaction with bone tissue under conditions of bone loss.

In this study, we therefore investigated the bones of the Djungarian hamster (Phodopus sungorus), a small photoperiod-sensitive mammal. Importantly, the changes in these animals are induced solely by environmental light–dark cues, without surgical or pharmacological intervention. We hypothesize that exposure to short-day photoperiods induces not only body weight loss but also a physiologically regulated reduction in bone volume. Specifically, we propose that this model of bone loss predominantly affects the trabecular compartment given its higher surface-to-volume ratio compared to cortical bone and results in reduced whole-bone structural and mechanical properties, while intrinsic bone material properties remain preserved. By characterizing these changes across cellular, structural, and mechanical scales, this work establishes the Djungarian hamster as a physiologically regulated model of bone loss that may serve as a future platform for investigating bone material adaptation in compromised skeletal environments and for informing endocrine mechanisms relevant to osteoanabolic strategies.

2. Materials and methods

2.1. Study design

Fifteen female Djungarian hamsters (*Phodopus sungorus*) were bred and raised at the Institute of Zoology, University of Hamburg (Reg.Nr. 9/2014, Hamburg, Germany). The animals, aged between three to four months were individually housed with free access to water and a hamster breeding diet (Altromin 7014, Germany) throughout the experiment. During the first 12–13 weeks, all animals were kept under long-day conditions (LD; 16:8 h light:dark cycle at 21 ± 1 °C ambient temperature). Subsequently, five hamsters remained in the LD cycle as controls, while 10 hamsters were transferred to short-day conditions (SD; 8:16 h light:dark cycle at 19 ± 1 °C), as shown in Fig. 1**A-B**.

After 14 weeks, all animals were euthanized by CO_2 inhalation and decapitated according to §4 of the German Animal Protection Law (18 May 2006, BGBI. I S.1207, 1313). Animals were euthanized under their respective housing light conditions (SD or LD) at 4 h after lights on (ZT4). SD-adapted animals were culled either during a torpor bout ($n = 5$) or on a day without torpor ($n = 5$). Torpor was determined by visual observation of the typical torpor posture at ZT4 and confirmed by a final body temperature measurement taken immediately after sacrifice. All animals in the SD groups experienced torpor during the experiment; however, not all were in torpor on the day of euthanasia. Body weights at the time of sacrifice are presented in Fig. 1**C**. Femora and tibiae were dissected, fixed in 3.7 % PBS-buffered formaldehyde for 24 h, and stored in 80 % ethanol. Subsequently, the mechanical, structural, and histomorphometric skeletal properties of the Djungarian hamsters were characterized, as illustrated in Fig. 1**D-F**.

2.2. Mechanical testing

Three-point bending tests were performed on the left femur following a previously established protocol, using a universal testing machine equipped with a 0 N to 200 N force sensor (Z.2.5/TN1S, Zwick/Roell, Ulm, Germany) [13–15]. Therefore, the femora were rehydrated in saline for two nights before being placed with the anterior surface facing up, on two cylindric bearing points, spaced 7 mm apart. Femurs were loaded perpendicularly to the midshaft with a rounded-off indenter lowered with a displacement rate of 0.5 mm/min until fracture. Load and displacement were detected, and maximum load (F_{max}, N), stiffness (K, N/mm), and work-to-fracture ($W_{fracture}$, N·mm) were calculated by the testing software (testXpert 10.1, Zwick/Roell, Ulm, Germany). Maximum stress (σ_{max}, $N{\cdot}mm^2$), maximum strain (ε_{max}) and Young's modulus (E_{mod}, kN/mm^2) were calculated using I_{min} (second moment of area about the axis of minimum bending stiffness) and c (distance from the neutral axis to the periosteal surface), both obtained from μCT analysis. Toughness was calculated by integrating the calculated stress–strain dataset using data analysis software (OriginPro 9, OriginLab Corporation, Northampton, MA, USA).

2.3. Microstructural analysis

Bone morphology and mineral content were assessed using micro-computed tomography (μCT). All scans were run with a 0.25 mm aluminum filter, a rotational step size of 0.2° over 180° and a frame averaging of 2 (Skyscan 1272, Bruker, Kontich, Belgium). Two phantoms with known concentrations of calcium hydroxyapatite (0.25 $g{\cdot}cm^{-3}$ and 0.75 $g{\cdot}cm^{-3}$) were scanned under the same conditions as the samples

to calibrate the scans for mineral content analysis. Consistent methods were applied to correct for ring artifacts and beam hardening during the reconstruction of scans of femora and tibiae in NRecon (Bruker, Kontich, Belgium).

To relate the morphological parameters and mineral content to mechanical tests, the cortex of the right femoral midshaft was analyzed in relation to the cortical diaphyseal region contralateral to the mechanical testing site. Therefore, femora were rehydrated in saline for two nights before scanning in a custom build sample holder wrapped in saline-soaked tissue. The femoral scans were acquired at 60 kV and 166 µA with a nominal isotropic resolution of 2.5 µm. For trabecular analysis, the proximal metaphysis of right tibiae were scanned in the same sample holder at 50 kV, 180 µA, and a nominal resolution of 5 µm.

The 3D bone morphology evaluation was conducted with CTAn (Bruker, Kontich, Belgium). For binarization of the bone, a common threshold was selected for each set of scans. For the cortical bone, a 3.5 mm long volume of interest (VOI) was set at the midshaft of the femur, excluding cancellous bone. The following morphological parameters were evaluated according to the nomenclature guideline of the American Society for Bone and Mineral research [16]: tissue mineral density ($TMD_{mean,}$ mgHA/ccm), cortical thickness (Ct.Th, mm), cortical porosity (Ct.Po, %), and marrow volume (Ma.V, mm^3).

In the tibiae, a 750 µm long VOI starting 300 µm below the growth plate was defined for trabecular analysis. Bone volume fraction (BV/TV, %), trabecular thickness (Tb.Th, mm), trabecular number (Tb.N, 1/mm) and trabecular separation (Tb.Sp, mm) were calculated [17].

2.4. Histomorphometric analysis

Left tibiae were dehydrated in an ascending alcohol series and embedded into polymethyl methacrylate (PMMA). Consecutive sections of 4 µm thickness were cut in the sagittal plane with a rotation microtome (microTec Laborgeräte GmbH, Walldorf/Baden, Germany) and stained with Toluidine Blue. Histomorphometry was carried out using the OsteoMeasure system (Osteometrics Inc., Atlanta, GA, USA) attached to a Carl Zeiss microscope (Carl Zeiss, Jena, Germany) [17]. The region of interest (ROI) was a square with a side length of 750 µm placed 300 µm below the growth plate next to the medial endocortical surface, only including trabecular bone. All analyses were performed at a magnification of x200. The following cellular indices were assessed: number of osteoblasts per bone perimeter (N.Ob/B.Pm, #/mm), osteoblast surface per bone surface (Ob.S/BS, %), number of osteocytes per bone area or total osteocyte lacunae density (Ot.Lc.Dn, $\#/mm^2$), number of viable osteocyte lacunae per bone area or full osteocyte lacunae density (fOt.Lc.Dn, $\#/mm^2$), and osteoclast surface per bone surface (Oc.S/BS, %), and erosion depth (E.De, µm) following ASBMR standards as described previously [17–19].

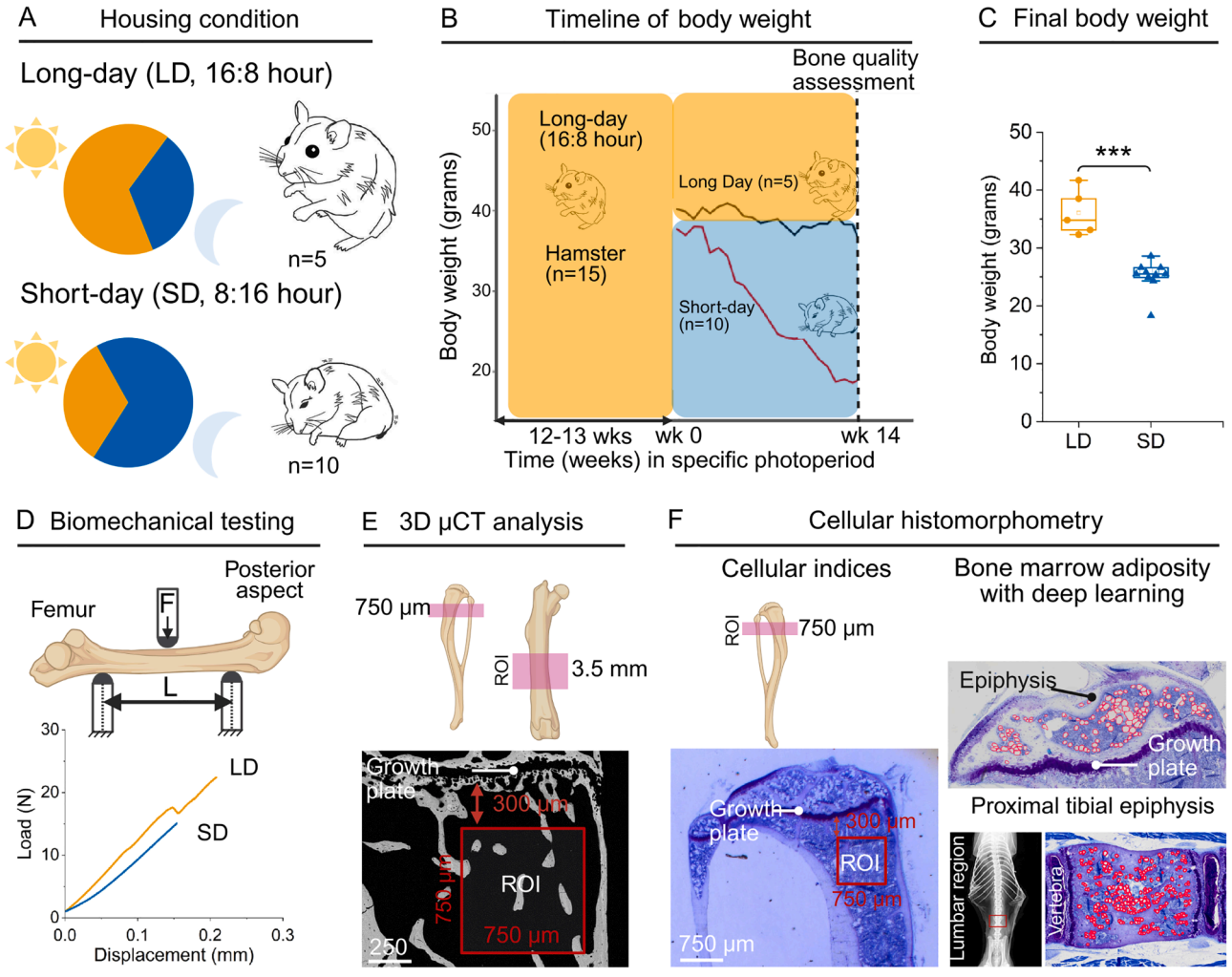

Fig. 1. Experimental design and methodology for studying bone characteristics in Djungarian hamsters. A) Experimental photoperiod housing conditions: exposure for 14 weeks. B) Weekly body weight changes under LD and SD conditions. C) Mean final body weight at the end of the experimental period. D). Schematic overview of the region of interest (ROI) for three-point bending, E) micro-computed tomography (µCT), and F) histomorphometry. ***$p < 0.001$.

2.5. Bone marrow adipocytes segmentation using deep learning

We trained a deep learning model to segment and quantify bone marrow adipocytes in images obtained by bone histomorphometry. For efficient training we reduced the image size by 50 % along the spatial axis. Further, to increase feature information due to the small size of bone marrow adipocytes (mean diameter 33.8 μm) and inference on large images we randomly cropped patches of size 1280 × 1280 pixels. We rejected crops if adipocytes were located partially close to the border to increase detection robustness. During training we applied data augmentations, e.g., flipping, rotations, scaling, hue, and brightness. As a basemodel we used YOLOv9-seg [20].

We manually annotated 17 images including both LD and SD groups, (epiphysis of tibia from LD: 4, and SD: 4 respectively, and vertebrae LD: 5, and SD: 4 respectively) using the online annotation tool CVAT. To evaluate the performance, we applied a 6-fold cross-validation by splitting the data set into a test, validation and training set (3–3–11 images). We iteratively defined a unique test set data during folds. We applied our model on full resolution images by cropping overlapping patches and defined an intersection over union of 0.5 and a detection score threshold of 0.5. We performed a 6-fold cross-validation and reported an overall precision of 0.919±0.038, recall of 0.702±0.088 and a mean average precision with threshold 0.5 of 0.819±0.059.

The following bone marrow adipocyte indices were assessed at the proximal tibial epiphysis (near the tibial growth plate) and lumbar vertebrae: bone area per tissue area (B.Ar/T.Ar, %), adipocyte area per marrow area (Ad.Ar/Ma.Ar, %), adipocyte area per bone area (Ad.Ar/B.Ar, %), adipocyte number per marrow area (N.Ad/Ma.Ar, #/μm^2), also known as adipocyte density, and mean adipocyte area (mean Ad.Ar, μm^2), which represents the mean size of adipocytes [21].

2.6. Statistical analysis

Statistical analysis was performed in SPSS statistical package, version 24. The Shapiro–Wilk test was performed to test for normality. In cases where the data followed a normal distribution, the Student's *t*-test was used, and for non-normally distributed data, the Mann–Whitney U test was utilized to analyze differences between groups. The significance level was set at $\alpha = 0.05$. A priori power analysis was performed before quantifying bone quality parameters, using changes in body weight and its standard deviation, as this was the only parameter available at the planning stage. For a two-tailed comparison with $\alpha = 0.05$, a group size of $n = 4$ was sufficient to achieve a statistical power of 0.95 (effect size = 3.243) based on the body weight distribution.

3. Results

3.1. Exposure to short-day light induces major metabolic changes in hamsters

The Djungarian hamsters lost 30.29 % of their body weight after 14 weeks of exposure to SD (LD: 36.08 ± 3.94 g, SD: 25.15 ± 2.68 g; $p \leq 0.001$). Uterus weight decreased by 48.21 % in the SD animals (LD: 0.17 ± 0.05 g; SD: 0.087 ± 0.02 g; $p \leq 0.001$). Terminal body temperature was 34.98 ± 0.50 °C for the LD animals ($n = 5$), 35.08 ± 0.40 °C for the SD animals culled on a day without torpor ($n = 5$) and 22.64 ± 0.40 °C for the SD animals sampled during a torpor bout ($n = 5$). Since no differences were detected in any bone quality parameters between the SD-with-torpor and SD-without-torpor groups prior to pooling, all SD animals were combined into a single group (SD).

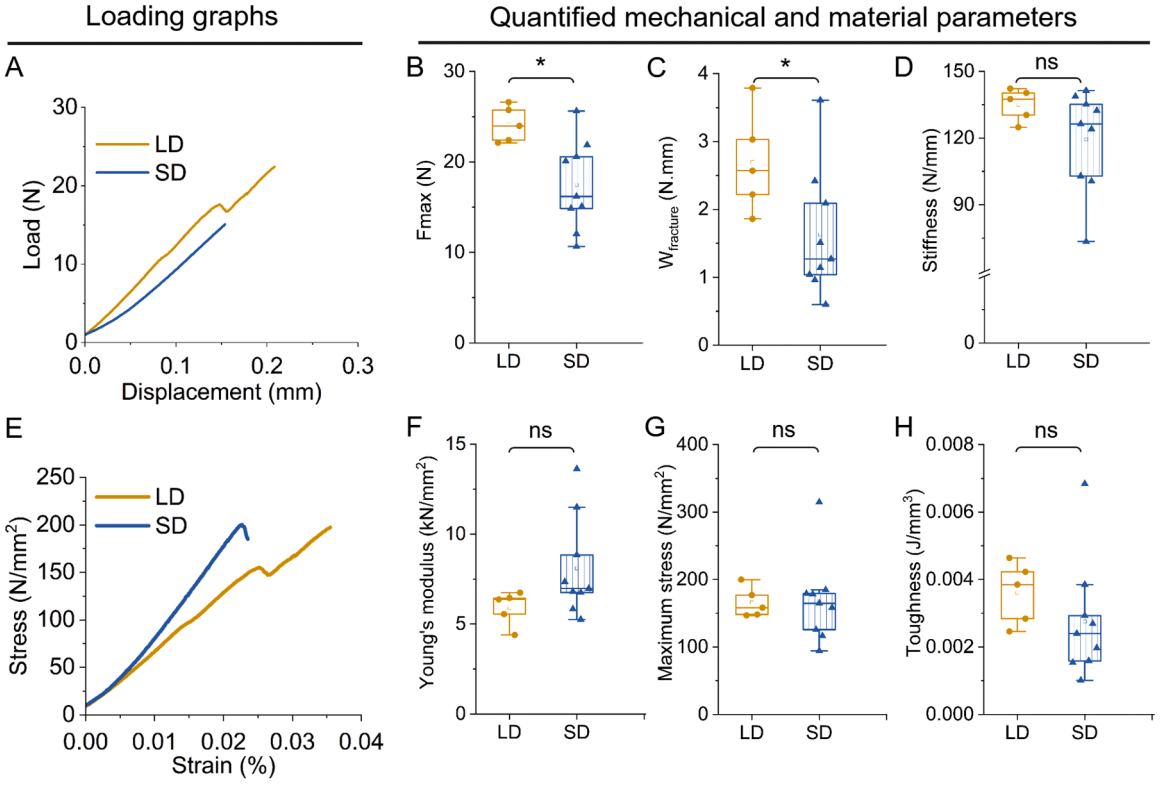

Fig. 2. Biomechanical properties of the femoral bone: A) Representative load–displacement curves obtained from three-point bending tests for LD and SD groups: Significantly lower maximum load (Fmax, B) and work-to-fracture ($W_{fracture}$, C) are observed in the SD group while stiffness (D) remains constant. E) Representative stress–strain curve derived from load-displacement data and normalized to bone morphological parameters obtained from μCT. No difference were observed in Young's modulus (F), maximum stress (G) or toughness (H) between the two groups. *$p < 0.05$, ns=not significant.

3.2. Mechanical strength is reduced by short-days

Three-point bending test revealed a lower maximum load (p = 0.013) and a lower work-to-fracture (p = 0.049) in the SD group compared with the LD group (Fig. 2**A-C**). No differences in stiffness were found between the groups (Fig. 2**D**). In both groups, very little to no plastic behavior was observed during the three-point bending tests. As a normalized material parameters: the Young's modulus, the maximum stress and toughness did not differ between the groups (Fig. 2**E-H**). The geometric parameters used for normalization of the mechanical results differed significantly between groups. SD animals showed a lower I_{min} (resistance to bending around the weakest axis, $p = 0.006$) and a lower c (distance from the centroid to the outer cortex, $p = 0.025$) compared with LD animals, mirroring reductions in cortical cross-sectional size and cortical thickness.

3.3. Short-days result in deteriorated trabecular and cortical bone microstructure

Tibia: The analysis of the trabecular bone (Fig. 3**A-B**) in the tibiae revealed a lower bone volume fraction ($p = 0.001$, Fig. 3**C**) in the SD group due to decreased trabecular number ($p = 0.003$, Fig. 3**D**) and lower trabecular thickness ($p = 0.023$, Fig. 3**E**). Accordingly, trabecular separation was higher in the SD group ($p = 0.017$, Fig. 3**F**).

Femur: In the diaphysis of the SD femora (Fig. 3**G-H**), a lower marrow volume (Fig. 3**I**) and lower cortical thickness (Fig. 3**J**) were measured in the SD group ($p < 0.003$ and $p = 0.009$, respectively). The cortical porosity (Fig. 3**K**) was lower in the SD group ($p < 0.001$). The analysis of the mineral content revealed a higher tissue mineral density (TMD_{mean}; $p = 0.004$) in the SD group compared to the LD-control group (Fig. 3**L**).

3.4. Cellular indices show signs of bone formation

The histomorphometric analysis revealed several distinct differences between the SD and LD groups. Osteoid with osteoblasts was detected on multiple trabeculae in the SD group, as seen in the representative image in Fig. 4**A**. In the LD group, no unmineralized tissue was observed. In agreement with this finding, a higher number of osteoblasts per bone perimeter ($p = 0.031$, Fig. 4**B**) and osteoblast surface per bone surface (p

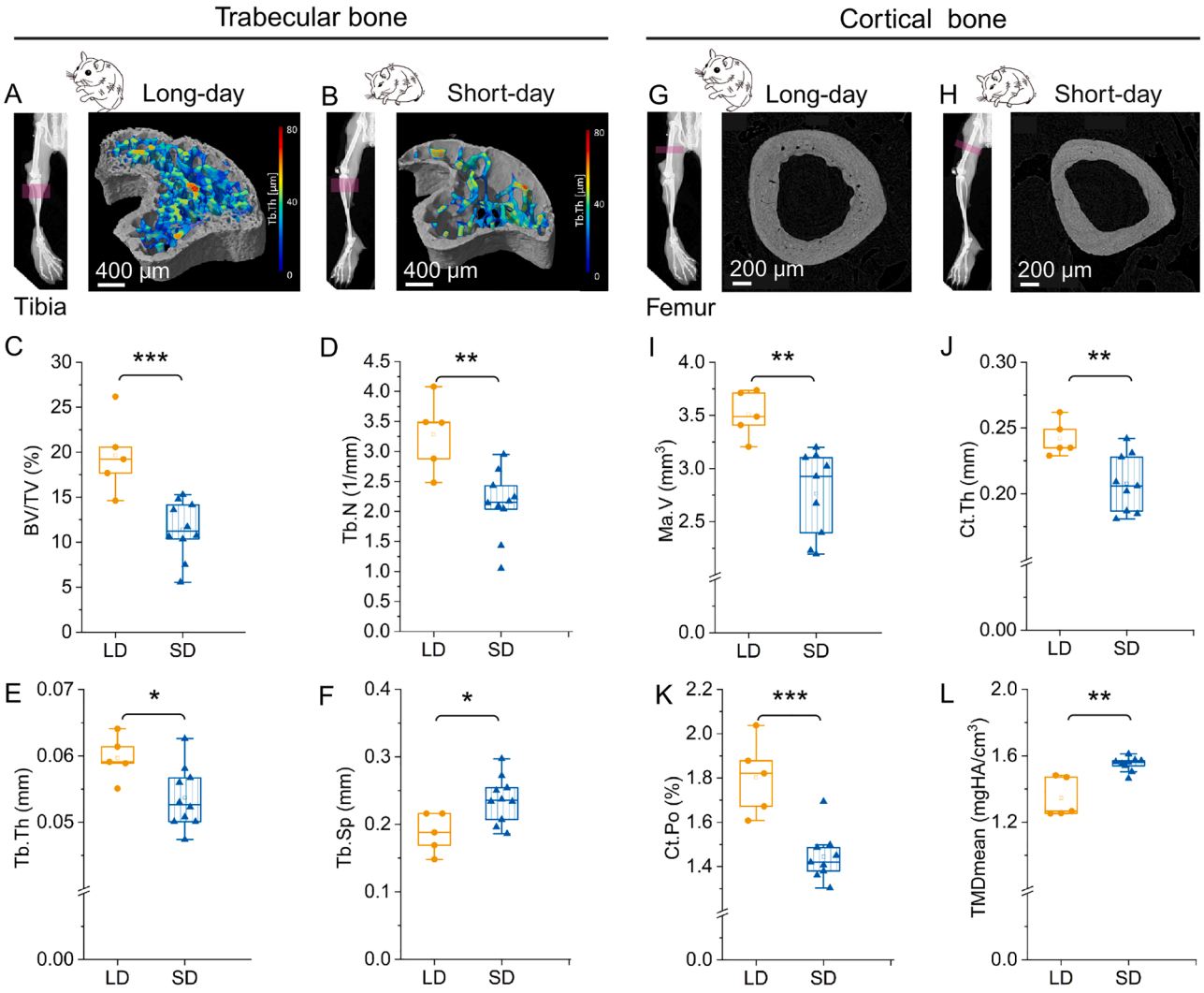

Fig. 3. Micro-computed tomography assessment of trabecular (A-F) and cortical (G-L) bone in Djungarian hamsters under LD and SD photoperiods. Representative µCT images of the proximal tibial trabecular bone from LD (A) and SD (B) groups. Color-coded overlays represent trabecular thickness (Tb.Th). Quantitative trabecular bone parameters derived from µCT analysis, including bone volume fraction (BV/TV, C), trabecular number (Tb.N, D), trabecular thickness (Tb.Th, E), and trabecular separation (Tb.Sp, F). Representative µCT cross-sections of femoral midshaft cortical bone from LD (G) and SD (H) groups. Quantitative cortical bone parameters, including marrow volume (Ma.V, I), cortical thickness (Ct.Th, J), cortical porosity (Ct.Po, K), and tissue mineral density (TMDmean, L). *$p < 0.05$, **$p < 0.01$, ***$p < 0.001$, ns=not significant.

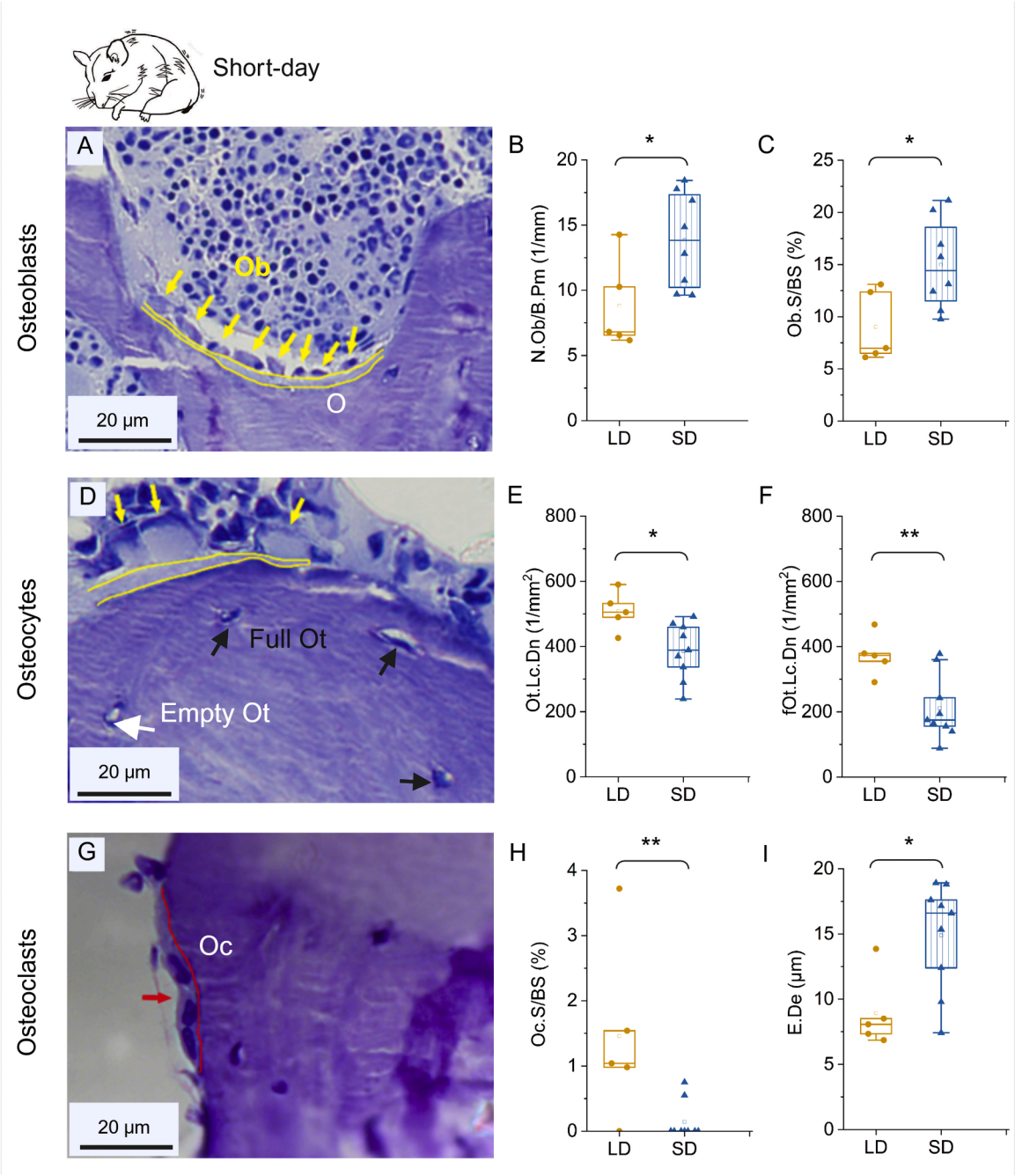

Fig. 4. Histomorphometric assessment of cellular indices in trabecular bone: A) Representative histological section showing osteoid (O, yellow line) with osteoblasts (Ob, yellow arrow), lining the trabecular surface in the SD group. B-C) Quantitative histomorphometric parameters of osteoblast activity, including osteoblast number per bone perimeter (N.Ob/B.Pm, B) and osteoblast surface per bone surface (Ob.S/BS, C) for the LD and SD groups. D) Representative image showing viable osteocytes (full Ot, black arrows) and empty osteocyte lacunae (empty Ot, white arrow). E-F) Quantification of total osteocyte lacunar density (Ot.Lc.Dn, E) and viable osteocyte lacunar density (fOt.Lc.Dn, F) in the LD and SD group. G) Representative image showing osteoclasts (Oc, red arrow) on the bone surface in the SD group. H, I) Quantitative osteoclast-related parameters, including osteoclast surface per bone surface (Oc.S/BS, H) and erosion depth (E.De, I), for the LD and SD group. *$p < 0.05$, **$p < 0.01$, ns=not significant. (For interpretation of the references to colour in this figure legend, the reader is referred to the web version of this article.)

= 0.023, Fig. 4**C**) were found in the SD group.

The full (viable) and empty osteocyte lacunae are shown in Fig. 4**D**. The total osteocyte lacunar density (Ot.Lc.Dn) was significantly lower in the SD samples ($p = 0.016$, Fig. 4**E**). The empty lacunae ($p = 0.374$) did not significantly differ between the groups, but the full (viable) osteocyte lacunar density was significantly lower in the SD group ($p = 0.006$, Fig. 4**F**).

Osteoclasts were scarce in both groups but were found more frequently in the LD group at the 14-week time point. While only 33 % of the SD samples showed osteoclasts, they were found in 80 % of the LD samples. A representative osteoclast in the SD group is shown in Fig. 4**G**. The resulting number of osteoclasts per bone perimeter ($p = 0.082$) and the osteoclast surface per bone surface ($p = 0.007$, Fig. 4**H**) were lower in the SD group. However, despite the lower presence of osteoclasts at week 14, the higher erosion depth in the SD group ($p = 0.020$, Fig. 4**I**) indicates that significant osteoclast activity occurred at some earlier

time point, contributing to the increased bone resorption seen in the SD group.

3.5. Adipocyte number increases due to short-days

The quantification of bone marrow adipocytes based on the deep learning approach revealed a lower bone area fraction in the SD group for the proximal tibial epiphysis ($p < 0.001$). The SD group also showed a higher adipocyte area per bone area and greater adipocyte number density in the proximal tibial epiphysis ($p = 0.004$ and $p = 0.003$ respectively) compared to the LD group. No differences were found in the average adipocyte size between groups (Fig. 5**A**). These findings suggest that new and additional adipocytes are formed in the bone marrow near the tibial growth plate in the SD group. In the vertebra, the SD group exhibited a lower bone area fraction ($p = 0.01$) and a smaller average adipocyte size ($p = 0.027$) compared to the LD group, but no differences were found in adipocyte number density (Fig. 5**B**).

4. Discussion

4.1. Bone material analytics in Djungarian hamster highlights photoperiod induced bone loss

This study proposes the Djungarian hamster as a natural, physiologically regulated model of accelerated bone loss induced solely by photoperiod manipulation. This model may enable future studies addressing drug development and the behavior of biomaterials in physiologically compromised bone under conditions of bone loss. Unlike traditional models that rely on invasive procedures (e.g., ovariectomy) or pharmacological interventions, this approach induces bone loss solely through endogenous physiological adaptations to SD photoperiods. Bone loss is accompanied by gonadal regression [8,12], reduced

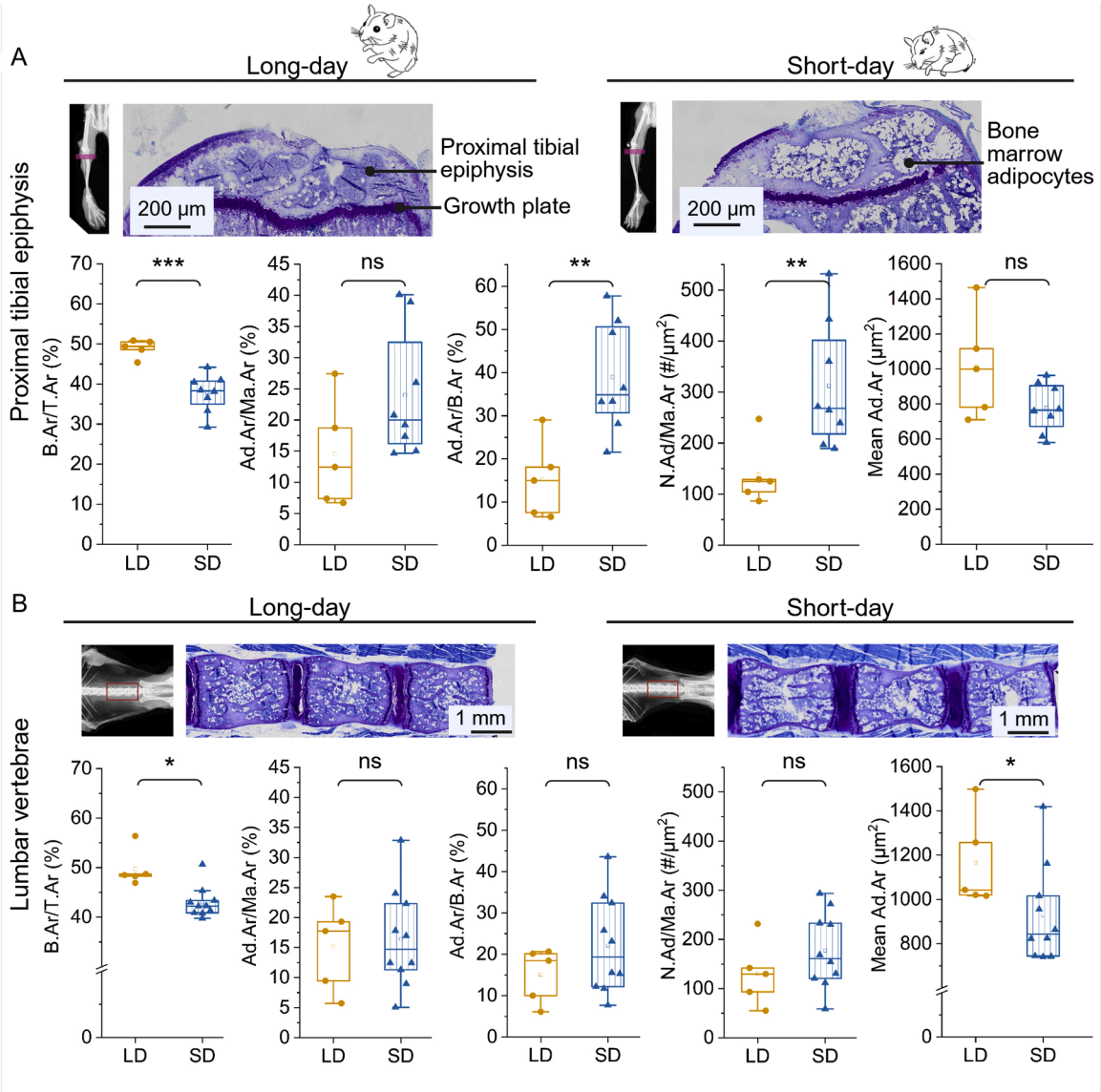

Fig. 5. Quantification of bone marrow adipocytes in the proximal tibial epiphysis and lumbar vertebrae: A) Representative histological sections of the proximal tibial epiphysis from LD (left) and SD (right) groups, showing bone marrow adipocytes in the region adjacent to the growth plate. The following quantitative parameters are measured (from left to right): bone area fraction (B.Ar/T.Ar), adipocyte area per marrow area (Ad.Ar/Ma.Ar), adipocyte area per bone area (Ad.Ar/B.Ar), adipocyte number density (N.Ad/Ma.Ar), and mean adipocyte area (Mean Ad.Ar). B) Representative histological sections of lumbar vertebrae from LD (left) and SD (right) groups. Corresponding quantitative parameters include (from left to right) bone area fraction (B.Ar/T.Ar), adipocyte area per marrow area (Ad.Ar/Ma.Ar), adipocyte area per bone area (Ad.Ar/B.Ar), adipocyte number density (N.Ad/Ma.Ar), and mean adipocyte area (Mean Ad.Ar). *$p < 0.05$, **$p < 0.01$, ***$p < 0.001$, ns=not significant.

physical activity [11], and other systemic changes [9], which together resemble key aspects of age-related osteoporosis in humans, including sarcopenia [22], reduced mobility [23,24], and decreased sex hormone levels [25].

The SD group exhibited significant deterioration in both trabecular and cortical bone compartments, as indicated by lower bone volume fraction (BV/TV), trabecular number, and cortical thickness. These changes were accompanied by decreased mechanical strength, observed through reductions in maximum load and work-to-fracture despite unchanged intrinsic material properties. This reduction in mechanical performance is attributable to alterations in bone architecture (bone mass loss as mirrored by reduced I_{min} and c), which diminish whole-bone structural properties, while intrinsic material properties of the remaining bone tissue remain preserved. Accordingly, normalization to geometry eliminates mass-driven differences, indicating maintained bone material quality despite reduced bone volume. This observed phenotype closely resembles human bone loss [23,24]. Therefore, the Djungarian hamster not only exhibits reduced body weight during torpor but also reduced bone mass as an adaptation to the SD cycle. While we have also reported in the formation of osteoid seams in the SD group, which are indicative of bone formation, these seams do not significantly influence the mechanical behavior given the soft matter.

4.2. Link between photoperiod changes to bone resorption

A significant increase in bone marrow adiposity was observed in the SD group, driven by higher adipocyte density. This mirrors findings in human conditions like osteoporosis [23,24] and energy-restricted states (e.g., anorexia nervosa) [26,27], where bone-fat trade-offs are influenced by systemic hormonal regulation. Concurrently, reductions in osteocyte lacunar density (decreasing material porosity) and increased erosion depth suggest localized bone resorption processes [28]. As cortical porosity under SD conditions was low, this suggests that resorptive processes are predominantly localized to bone regions characterized by high surface area i.e. higher osteocyte density, higher porosity (i.e. endocortical [29,30]) and lower mineral content. These findings highlight that bone compartments with large surface-to-volume ratios may serve as primary sites of bone resorption. This underscores the importance of porosity and mineral content as critical parameters influencing bone quality and resorption: highly porous, low mineralized bone is more susceptible to resorption processes and therefore is reduced more rapidly (such as in comparing LD to SD transition), whereas low porosity bone tends to remain as the denser residual bone in case of reduced bone mass with high mineral content [31,32]. These cellular and structural changes are consistent with a photoperiod-regulated remodeling response in which circadian and endocrine mechanisms shift bone turnover toward resorption. Prolonged melatonin signaling [33], reduced sex hormone levels, as reflected by gonadal regression [12], and decreased skeletal loading under SD conditions are all conditions known to promote osteoclast activity and impair osteocyte viability in other animal models and humans [11,24]. Together, these observations provide a plausible mechanistic link between photoperiod changes and bone mass reduction. Thus, understanding the interaction between endocrine signaling, reduced mechanical loading during torpor, and altered energy intake may help to inform the development of future therapeutic strategies targeting osteoporosis.

4.3. Signs of bone formation in short-day animals may be indicative of possible reversibility of bone loss

Interestingly, localized increases in osteoid volume suggest early signs of bone formation, indicating that this model may capture early features associated with bone formation processes that have been linked to recovery phases in other species, including humans [34]. The presence of osteoid seams matches the increased osteoblast number, potentially driven by endocrine mechanisms priming the skeleton for renewed bone formation; however, this interpretation remains hypothetical, as endocrine parameters were not assessed in the present study. Importantly, the detection of osteoblast-associated osteoid under SD conditions argues against a purely irreversible, resorptive state and instead suggests the presence of localized bone formation activity within an otherwise resorptive state. This interpretation is consistent with the well-described regain of body weight following prolonged SD exposure in Djungarian hamsters [8]. Given the physiological regulation of bone loss in the Djungarian hamster, this model may be of particular interest for studying biomaterial performance and stability in compromised skeletal environments, as commonly encountered in elderly patients receiving orthopedic implants, where stability and bone–implant interactions are compromised. Importantly, it also provides a conceptual framework to explore how changes in skeletal loading and physiological state [35], may influence biomaterial behavior in future studies, without reliance on pharmacological intervention.

4.4. Limitations

This study has limitations. Its cross-sectional design prevented longitudinal tracking of bone changes within the same animals. Baseline skeletal measurements were not assessed, requiring reliance on age- and sex-matched controls and averaged morphological data may not fully capture site-specific variations. As well, hormonal levels have not been assessed within this study. Although a regain of body weight after SD photoperiods suggests potential reversibility of bone mass [8], this was not directly assessed in our study; therefore, reversibility cannot be conclusively demonstrated based on the present data.

As this is the first study to link photoperiod manipulations with bone changes in Djungarian hamsters, the underlying mechanism of bone loss is primarily circadian and photoperiod-driven, involving coordinated endocrine, metabolic, and mechanical-loading changes that occur concurrently in this model. As these processes are tightly interrelated, their individual contributions were not dissected in the present study. Finally, although the model holds strong potential for investigating bone–biomaterial interactions, biomaterials or implants were not tested in this study, and these applications remain to be explored in future work.

4.5. Translational relevance of the Djugarian hamster model for biomaterials

Despite limitations, the Djungarian hamster provides a unique, non-surgical model for studying bone loss. It offers opportunities to evaluate how altered bone geometry, microarchitecture, and marrow composition influence mechanical performance and may inspire the design of biomaterials or scaffolds capable of supporting osteoanabolic treatments or maintaining functionality in low-bone-mass environments. The model bridges a critical gap between preclinical biomaterial testing in healthy bone and clinical scenarios involving physiologically or pathologically compromised skeletal tissue. Importantly, the Djungarian hamster model resembles key features of postmenopausal osteoporosis beyond bone mass reduction. These include body weight loss [8], loss of muscle mass and physical activity [11], features consistent with osteosarcopenia observed in postmenopausal patients [22], as well as age-related reductions in mechanical loading [24] accompanied by shifts in sex hormone levels [36].

5. Conclusions

The Djungarian hamster represents a natural, non-invasive, and physiologically regulated model of accelerated bone loss driven solely by photoperiod changes. Short-day-induced bone loss resembles key features of human skeletal compromise, including reductions in trabecular and cortical structure, diminished whole-bone mechanical competence, and increased marrow adiposity, while intrinsic bone

material properties remain preserved. This model provides a physiologically relevant framework to study skeletal adaptation, endocrine regulations, and the interplay between bone geometry, microstructure, and mechanics. Moreover, it establishes a foundation for future investigation into bone-biomaterial interactions and osteoanabolic strategies under conditions that more closely reflect human physiological bone loss than traditional surgical or pharmacological models. Collectively, the photoperiod-induced Djungarian hamster model holds strong potential as a valuable tool for both fundamental bone biology and preclinical biomaterials research.

Data availability

Data can be made available upon reasonable request.

CRediT authorship contribution statement

Felix N. von Brackel: Writing – original draft, Visualization, Validation, Supervision, Methodology, Investigation, Formal analysis, Data curation. **Praveer Sihota:** Writing – review & editing, Visualization, Validation, Supervision, Methodology, Investigation, Formal analysis, Data curation. **Kathrin Mletzko:** Software, Methodology, Investigation, Formal analysis, Data curation. **Johannes van Kaick:** Software, Investigation, Formal analysis. **Johannes Krug:** Visualization, Methodology, Investigation. **Xenia Junimann:** Software, Investigation, Formal analysis. **Ceyda Cubuk-Charalampous:** Methodology, Data curation. **Maximilian Neidhardt:** Writing – review & editing, Software, Methodology, Data curation. **Alexander Schlaefer:** Writing – review & editing, Resources. **Petar Milovanovic:** Writing – review & editing, Visualization. **Annegreet Vlug:** Writing – review & editing, Validation. **Katharina Jähn-Rickert:** Writing – review & editing, Visualization, Validation, Supervision, Project administration, Methodology, Investigation. **Annika Herwig:** Writing – review & editing, Resources, Project administration, Funding acquisition, Conceptualization. **Björn Busse:** Writing – review & editing, Visualization, Resources, Project administration, Funding acquisition, Conceptualization.

Declaration of competing interest

The authors declare that they have no known competing financial interests or personal relationships that could have appeared to influence the work reported in this paper.

Acknowledgements

FvB, BB, CCC and AH acknowledge funding from the Deutsche Forschungsgemeinschaft (German Research Foundation) [grant number SCHM 3777/1 (FvB), BU2562-10/1 (BB), HE6383/1 (CCC AH)]. PS is supported by a postdoctoral fellowship from the Alexander von Humboldt Foundation. PM acknowledges support from the Ministry of Science of the Republic of Serbia (Center of Bone Biology as a Center of Excellence) and Science Fund of the Republic of Serbia [grant BoFraM]. PM and BB also thank the Interinstitutional Partnership Program of the Alexander von Humboldt Foundation.

References

[1] M. Fini, G. Giavaresi, P. Torricelli, V. Borsari, R. Giardino, A. Nicolini, A. Carpi, Osteoporosis and biomaterial osteointegration, Biomed. PharmacOther 58 (2004) 487–493, https://doi.org/10.1016/j.biopha.2004.08.016.

[2] K.D. Anderson, F.C. Ko, A.S. Virdi, D.R. Sumner, R.D. Ross, Biomechanics of implant fixation in osteoporotic bone, Curr. Osteoporos. Rep. 18 (2020) 577–586, https://doi.org/10.1007/s11914-020-00614-2.

[3] N.M. Appelman-Dijkstra, H.L.D.W. Oei, A.G. Vlug, E.M. Winter, The effect of osteoporosis treatment on bone mass, Best Pr. Res. Clin. Endocrinol. Metab. 36 (2022) 101623, https://doi.org/10.1016/j.beem.2022.101623.

[4] M.R. McClung, M.S. Rothman, E.M. Lewiecki, D.A. Hanley, S.T. Harris, P.D. Miller, D.L. Kendler, The role of osteoanabolic agents in the management of patients with osteoporosis, Postgr. Med. 134 (2022) 541–551, https://doi.org/10.1080/00325481.2022.2069582.

[5] M.A. Bredella, P.K. Fazeli, K.K. Miller, M. Misra, M. Torriani, B.J. Thomas, R. H. Ghomi, C.J. Rosen, A. Klibanski, Increased bone marrow fat in anorexia nervosa, J. Clin. Endocrinol. Metab. 94 (2009) 2129–2136, https://doi.org/10.1210/jc.2008-2532.

[6] I. Daniilopoulou, E. Vlachou, G.I. Lambrou, A. Ntikoudi, E. Dokoutsidou, G. Fasoi, O. Govina, A. Kavga, A.N. Tsartsalis, The impact of GLP1 agonists on bone metabolism: a systematic review, Medicines 58 (2022) 1–13, https://doi.org/10.3390/medicina58020224.

[7] J. Paccou, E. Tsourdi, C. Meier, A. Palermo, J. Pepe, J.J. Body, M.C. Zillikens, Bariatric surgery and skeletal health: a narrative review and position statement for management by the European Calcified Tissue Society (ECTS), Bone 154 (2022) 116236, https://doi.org/10.1016/j.bone.2021.116236.

[8] A. Herwig, E.M. de Vries, M. Bolborea, D. Wilson, J.G. Mercer, F.J.P. Ebling, P. J. Morgan, P. Barrett, Hypothalamic ventricular ependymal thyroid hormone deiodinases are an important element of circannual timing in the Siberian hamster (Phodopus sungorus), PLoS. One 8 (2013), https://doi.org/10.1371/journal.pone.0062003.

[9] F. Scherbarth, S. Steinlechner, Endocrine mechanisms of seasonal adaptation in small mammals: from early results to present understanding, J. Comp. Physiol. B Biochem. Syst. Env. Physiol. 180 (2010) 935–952, https://doi.org/10.1007/s00360-010-0498-2.

[10] A.K. Kissmann, F. Rosenau, A. Herwig, V. Diedrich, Short photoperiod-dependent enrichment of Akkermansia spec. As the major change in the intestinal microbiome of Djungarian hamsters (Phodopus sungorus), Int. J. Mol. Sci. 24 (2023), https://doi.org/10.3390/ijms24076605.

[11] M.E. McGee-Lawrence, H.V. Carey, S.W. Donahue, Mammalian hibernation as a model of disuse osteoporosis: the effects of physical inactivity on bone metabolism, structure, and strength, Am. J. Physiol. - Regul. Integr. Comp. Physiol. 295 (2008), https://doi.org/10.1152/ajpregu.90648.2008.

[12] C.S. Moffatt-Blue, J.J. Sury, K.A. Young, Short photoperiod-induced ovarian regression is mediated by apoptosis in Siberian hamsters (Phodopus sungorus), Reproduction 131 (2006) 771–782, https://doi.org/10.1530/rep.1.00870.

[13] K.J. Jepsen, M.J. Silva, D. Vashishth, X.E. Guo, M.C.H. Van Der Meulen, Establishing biomechanical mechanisms in mouse models: practical guidelines for systematically evaluating phenotypic changes in the diaphyses of long bones, J. Bone Min. Res. 30 (2015) 951–966, https://doi.org/10.1002/jbmr.2539.

[14] M. Schilperoort, N. Bravenboer, J. Lim, M. Kathrin, B. Busse, Circadian disruption by shifting the light-dark cycle negatively affects bone health in mice, FASEB J. 34 (2020) 1052–1064, https://doi.org/10.1096/fj.201901929R.

[15] P. Sihota, R.N. Yadav, S. Poleboina, V. Mehandia, S.K. Bhadada, K. Tikoo, N. Kumar, Development of HFD -fed/low dose STZ treated female Sprague Dawley rat model to investigate diabetic bone fragility at different organization levels, JBMR. Plus. (2020), https://doi.org/10.1002/jbm4.10379.

[16] M.L. Bouxsein, S.K. Boyd, B.A. Christiansen, R.E. Guldberg, K.J. Jepsen, R. Müller, Guidelines for assessment of bone microstructure in rodents using micro-computed tomography, J. Bone Min. Res. 25 (2010) 1468–1486, https://doi.org/10.1002/jbmr.141.

[17] D.W. Dempster, J.E. Compston, M.K. Drezner, F.H. Glorieux, J.A. Kanis, H. Malluche, P.J. Meunier, S.M. Ott, R.R. Recker, A.M. Parfitt, Standardized nomenclature, symbols, and units for bone histomorphometry: a 2012 update of the report of the ASBMR Histomorphometry Nomenclature Committee, J. Bone Min. Res. 28 (2013) 2–17, https://doi.org/10.1002/jbmr.1805.

[18] E.M. Wölfel, K. Jähn-Rickert, F.N. Schmidt, B. Wulff, H. Mushumba, G.E. Sroga, K. Püschel, P. Milovanovic, M. Amling, G.M. Campbell, D. Vashishth, B. Busse, Individuals with type 2 diabetes mellitus show dimorphic and heterogeneous patterns of loss in femoral bone quality, Bone 140 (2020) 115556, https://doi.org/10.1016/j.bone.2020.115556.

[19] B. Jobke, P. Milovanovic, M. Amling, B. Busse, Bisphosphonate-osteoclasts: changes in osteoclast morphology and function induced by antiresorptive nitrogen-containing bisphosphonate treatment in osteoporosis patients, Bone 59 (2014) 37–43, https://doi.org/10.1016/j.bone.2013.10.024.

[20] C.-Y. Wang, I.-H. Yeh, H.-Y.M. Liao, YOLOv9: learning what you want to learn using programmable gradient information, (2024). doi:10.48550/arXiv.2402.13616.

[21] N. Bravenboer, M.A. Bredella, C. Chauveau, A. Corsi, E. Douni, W.F. Ferris, M. Riminucci, P.G. Robey, S. Rojas-Sutterlin, C. Rosen, T.J. Schulz, W.P. Cawthorn, Standardised nomenclature, abbreviations, and units for the study of Bone Marrow Adiposity: report of the Nomenclature Working Group of the International Bone Marrow Adiposity Society, Front. Endocrinol. 10 (2020) 1–21, https://doi.org/10.3389/fendo.2019.00923.

[22] A. Simon;, H.S. Schäfer, F.N. Schmidt, J. Stürznickel, M. Amling, T. Rolvien, Compartment-specific effects of muscle strength on bone microarchitecture in women at high risk of osteoporosis, J. Cachexia Sarcopenia Muscle 13 (2022) 2310–2321, https://doi.org/10.1002/jcsm.13044.

[23] G.J. Kazakia, W. Tjong, J.A. Nirody, A.J. Burghardt, J. Carballido-Gamio, J. M. Patsch, T. Link, B.T. Feeley, C.B. Ma, The influence of disuse on bone microstructure and mechanics assessed by HR-pQCT, Bone 63 (2014) 132–140, https://doi.org/10.1016/j.bone.2014.02.014.

[24] T. Rolvien, M. Amling, Disuse osteoporosis: clinical and mechanistic insights, Calcif. Tissue Int. 110 (2022) 592–604, https://doi.org/10.1007/s00223-021-00836-1.

[25] A.S. Karlamangla, S.-A.M. Burnett-Bowie;, C.J. Crandall, Bone health during the menopause transition and beyond, Physiol. Behav. 176 (2018) 139–148, https://doi.org/10.1016/j.ogc.2018.07.012.

[26] M. Lorentzon, H. Johansson, N.C. Harvey, E. Liu, L. Vandenput, E.V. McCloskey, J. A. Kanis, Osteoporosis and fractures in women: the burden of disease, Climacteric. 25 (2022) 4–10, https://doi.org/10.1080/13697137.2021.1951206.

[27] I. Legroux, B. Cortet, Factors influencing bone loss in anorexia nervosa: assessment and therapeutic options, RMD. Open. 5 (2019) 1–8, https://doi.org/10.1136/rmdopen-2019-001009.

[28] P. Milovanovic, E.A. Zimmermann, M. Hahn, D. Djonic, K. Püschel, M. Djuric, M. Amling, B. Busse, Osteocytic canalicular networks: morphological implications for altered mechanosensitivity, ACS. Nano 7 (2013) 7542–7551, https://doi.org/10.1021/nn401360u.

[29] C.M. Andreasen, L.P. Bakalova, A. Brüel, E.M. Hauge, B.J. Kiil, J.M. Delaisse, M. E. Kersh, J.S. Thomsen, T.L. Andersen, The generation of enlarged eroded pores upon existing intracortical canals is a major contributor to endocortical trabecularization, Bone 130 (2020) 115127, https://doi.org/10.1016/j.bone.2019.115127.

[30] G. Ziervogel, A. Cartwright, A. Tas, J. Adejuwon, F. Zermoglio, M. Shale, B. Smith, Endocortical bone loss in osteoporosis: the role of bone surface availability, in: 2013: pp. 1307–1322. doi:10.1002/cnm.

[31] T. Rolvien, P. Milovanovic, F.N. Schmidt, S. von Kroge, E.M. Wölfel, M. Krause, B. Wulff, K. Püschel, R.O. Ritchie, M. Amling, B. Busse, Long-term immobilization in elderly females causes a specific pattern of cortical bone and osteocyte deterioration different from postmenopausal osteoporosis, J. Bone Min Res. 35 (2020) 1343–1351, https://doi.org/10.1002/jbmr.3970.

[32] W.K. Sietsema, Animal models of cortical porosity, Bone 17 (1995) 297–305, https://doi.org/10.1016/8756-3282(95)00307-Y.

[33] M.R. Gorman, Independence of circadian entrainment state and responses to melatonin in male Siberian hamsters, BMC. Physiol. 3 (2003) 1–11, https://doi.org/10.1186/1472-6793-3-1.

[34] J.M. Delaisse, T.L. Andersen, H.B. Kristensen, P.R. Jensen, C.M. Andreasen, K. Søe, *Re*-thinking the bone remodeling cycle mechanism and the origin of bone loss, Bone 141 (2020) 115628, https://doi.org/10.1016/j.bone.2020.115628.

[35] H.C. Cunningham, D.W.D. West, L.M. Baehr, F.D. Tarke, K. Baar, S.C. Bodine, B. A. Christiansen, Age-dependent bone loss and recovery during hindlimb unloading and subsequent reloading in rats, BMC. Musculoskelet. Disord. 19 (2018) 1–11, https://doi.org/10.1186/s12891-018-2156-x.

[36] X. Tian, B. Zhang, The association between sex hormones and bone mineral density in US females, Sci. Rep. 15 (2025) 1–10, https://doi.org/10.1038/s41598-025-89985-z.